Monthly Notices
of the
ROYAL ASTRONOMICAL SOCIETY

Mon. Not. R. Astron. Soc. **402,** 2397–2402 (2010) doi:10.1111/j.1365-2966.2009.15903.x

The non-linear redshift space probability distribution function in models with local primordial non-Gaussianity

Tsz Yan Lam,[1,2⋆] Vincent Desjacques[3⋆] and Ravi K. Sheth[1⋆]

[1] *Center for Particle Cosmology, University of Pennsylvania, 209 S. 33rd Street, Philadelphia, PA 19104, USA*
[2] *Institute for the Physics and Mathematics of the Universe, University of Tokyo, Kashiwa, Chiba 277-8568, Japan*
[3] *Institute for Theoretical Physics, University of Zürich, Winterthurerstrasse 190, CH-8057 Zürich, Switzerland*

Accepted 2009 October 20. Received 2009 October 19; in original form 2009 August 17

ABSTRACT

We use the ellipsoidal collapse approximation to investigate the non-linear redshift space evolution of the density field with primordial non-Gaussianity of the local $f_{\rm nl}$-type. We utilize the joint distribution of eigenvalues of the initial non-Gaussian shear field and evaluate the evolved redshift space probability distribution function (PDF). It is shown that, similar to the real space analysis, the underdense tail of the non-linear redshift space PDF differs significantly from that for Gaussian initial conditions. We also derive the lowest order correction of the Kaiser's formula in the presence of a non-zero $f_{\rm nl}$.

Key words: methods: analytical – dark matter – large-scale structure of Universe.

1 INTRODUCTION

Cosmological probes of primordial non-Gaussianity have recently attracted much attention because of their potential ability to discriminate between different inflationary models (e.g. Buchbinder, Khoury & Ovrut 2008; Khoury & Piazza 2009; Silvestri & Trodden 2008, and references therein). Constraints on primordial non-Gaussianity mainly come from the cosmic microwave background (Hikage et al. 2008; McEwen et al. 2008; Yadav & Wandelt 2008; Komatsu et al. 2009; Rossi et al. 2009) and large-scale structures in the Universe (Koyama, Soda & Taruya 1999; Matarrese, Verde & Jimenez 2000; Scoccimarro, Sefusatti & Zaldarriaga 2004; Sefusatti & Komatsu 2007; Izumi & Soda 2007; Lo Verde et al. 2008; Dalal et al. 2008; Matarrese & Verde 2008; Carbone, Verde & Matarrese 2008; Afshordi & Tolley 2008; Slosar et al. 2008; McDonald 2008; Taruya, Koyama & Matsubara 2008; Slosar 2009; Grossi et al. 2008; Kamionkowski, Verde & Jimenez 2009; Desjacques, Seljak & Iliev 2009; Pillepich, Porciani & Hahn 2008; Lam & Sheth 2009; Grossi et al. 2009; Lam, Sheth & Desjacques 2009).

This paper is concerned with one particular measure of large-scale structures: the probability that a cell of volume V, placed at random in the non-linear redshift space density field, contains a certain amount of mass (or, equivalently, is denser than the background by a certain amount). This statistic is known as the non-linear redshift space probability distribution function (PDF). Our goal is to estimate this distribution for scales as small as a few Mpc in the local non-Gaussian model, in which the primordial perturbation potential is

$$\Phi = \phi + f_{\rm nl}(\phi^2 - \langle\phi^2\rangle). \quad (1)$$

Here, Φ is the Bardeen potential, ϕ is a Gaussian potential field and $f_{\rm nl}$ is the non-linear quadratic parameter. The right-hand side of equation (1) shows the first two terms of an (infinite) Taylor series in ϕ. However, since $|\phi| \sim 10^{-5}$, one usually ignores higher order corrections and commonly refers to this simplified model as the $f_{\rm nl}$ model. This definition of Φ is consistent with most of the recent studies on the local $f_{\rm nl}$ model (but our earlier studies, Lam & Sheth 2009; Lam et al. 2009, defined Φ as the Newtonian potential).

Our approach is based on previous work which develops the formalism needed for estimating the evolution of the density PDF from Gaussian initial conditions in real and redshift space (Lam & Sheth 2008a,b). The evolved PDF depends on the collapse dynamics and the statistical properties of the initial density field. Recently, Lam & Sheth (2009) used the fact that only the initial conditions are affected by primordial non-Gaussianity to model the evolution of the real space non-linear PDF for the local non-Gaussian model. Their approach provided good quantitative agreement with measurements in numerical simulations. In what follows, we will assess whether this is also true in redshift space.

Although it is possible to study the evolution of the redshift space PDF using perturbation theory methods (Bernardeau 1994; Hivon et al. 1995; Scoccimarro & Frieman 1999; Bernardeau et al. 2002), this has, somewhat surprisingly not been extended to the local non-Gaussian model. Thus, it is not obvious how Kaiser's formula relating the variance (the second moment of the PDF) in real and redshift space (Kaiser 1987) is modified when the initial conditions are non-Gaussian. Although Kaiser's original derivation makes no explicit assumption about Gaussianity, the Gaussian assumption plays an important role in other derivations of his

⋆E-mail: tszyan.lam@ipmu.jp (TYL); dvince@physik.uzh.ch (VD); shethrk@physics.upenn.edu (RKS)

formula (e.g. Fisher 1995; Ohta et al. 2004). Our approach is quite different from Kaiser's, as it is based on an approximate model for the dynamics – the ellipsoidal collapse model – which reduces to perturbation theory at early times (Bond & Myers 1996), but allows one to study more non-linear structures (Sheth, Mo & Tormen 2001; Desjacques 2008). Lam & Sheth (2008b) showed that the ability to probe deeper into the non-linear regime, using a dynamical model that does *not* assume spherical symmetry, was crucial for modelling the PDF, especially in redshift space. However, implementing this approach requires knowledge of the initial shear field. For Gaussian initial conditions, this has been known for some time (Doroshkevich 1970), but how Doroshkevich's formulae are modified for the local $f_{\rm nl}$ model has been shown only recently (Lam et al. 2009). Hence, we now have the necessary ingredients to study the redshift space PDF.

Properties of the initial shear field in the local non-Gaussian model are briefly reviewed in Section 2.1. The dynamics of ellipsoidal collapse and the calculation of the non-linear redshift space PDF are described in Sections 2.2 and 2.3. We compare our model predictions with numerical simulations in Section 3. We summarize our results in Section 4. A perturbative treatment of our model is given in Appendix A; this shows explicitly that Kaiser's formula holds to the lowest order in $f_{\rm nl}$, but that at higher order, it is modified.

2 THE REDSHIFT SPACE DENSITY PDF IN THE LOCAL NON-GAUSSIAN MODEL

Let us define the non-linear overdensity of a region of volume V containing mass M by

$$\rho \equiv 1 + \delta = \frac{M}{\bar{\rho} V}, \tag{2}$$

where $\bar{\rho}$ is the mean density. We will use ρ_s to denote the corresponding quantity in redshift (rather than real) space. This section studies the expected dependence of the PDF of ρ_s on the value of $f_{\rm nl}$, when the primordial potential is given by equation (1).

To proceed, we use the assumptions made when dealing with Gaussian initial distributions ($f_{\rm nl} = 0$): there is a local mapping from the eigenvalues λ_j of the initial deformation tensor to the non-linear overdensity ρ_s (see Section 2.2), and statistics on the smoothing scale V at the present time are related to statistics on a different smoothing scale in the initial conditions – the relevant initial smoothing scale is the one which contains the same mass (so it is larger for overdense cells, and smaller for underdense cells).

Therefore, the non-linear redshift space PDF of ρ_s is given by

$$\rho_s\, p(\rho_s|V) {\rm d}\rho_s = \int {\rm d}\boldsymbol{\lambda}\, {\rm d}\boldsymbol{e}\; p(\boldsymbol{\lambda}|\sigma)\, \delta_{\rm D}\left[\rho_s = \rho_s'(\boldsymbol{\lambda}, \boldsymbol{e})\right], \tag{3}$$

where $\rho_s \equiv M/\bar{M} (\bar{M} \equiv \bar{\rho} V$ is the average mass in cells of size V), λ denotes the three eigenvalues (our convention is to have $\lambda_1 \geq \lambda_2 \geq \lambda_3$) of the initial 3×3 deformation tensor when smoothed on scale M (not V), σ^2 denotes the variance of the initial density fluctuation field on this smoothing scale (the initial density fluctuation δ_l is defined by $\delta_l \equiv {\rm Tr}\,\boldsymbol{\lambda}$), $\rho_s'(\boldsymbol{\lambda}, \boldsymbol{e})$ is the local mapping from the initial field to the evolved density given by the ellipsodial collapse model (spherical evolution models assume that the mapping is driven by the initial density δ_l only) and $\boldsymbol{e}$ represents the rotation vector from the line-of-sight direction to the principle axis of the ellipsoid. Equation (3) has the same form as equation (8) of Lam & Sheth (2008b) but, in our case, $p(\boldsymbol{\lambda}|\sigma)$ is the joint distribution of the initial eigenvalues λ_j in the $f_{\rm nl}$ model rather than in the Gaussian model.

Before we compute $p(\boldsymbol{\lambda}|\sigma)$, note that equation (3) does not guarantee a properly normalized PDF. To ensure the correct normalization, we set $\rho' = N\rho$ and $\rho'^2\; p(\rho') = \rho^2 p(\rho)$ where N is chosen so that both $\int {\rm d}\rho'\; p(\rho')$ and $\int {\rm d}\rho'\; \rho' p(\rho')$ equal unity (Lam & Sheth 2008a).

2.1 Initial conditions in the $f_{\rm nl}$ model

Let $p(\boldsymbol{\lambda}|\delta_l, \sigma)$ denote the distribution of the λ_j at fixed δ_l, and let $p_0(\boldsymbol{\lambda}|\sigma)$ and $p_0(\boldsymbol{\lambda}|\delta_l, \sigma)$ denote the corresponding quantities when $f_{\rm nl} = 0$, i.e. for Gaussian initial conditions. [Note that this means $p_0(\delta_l)$ is a Gaussian.] One of the main results of Lam et al. (2009) was to show that

$$\begin{aligned} p(\boldsymbol{\lambda}|\delta_l, \sigma) &= p_0(\boldsymbol{\lambda}|\delta_l, \sigma) \\ &= \frac{3^4/4}{\Gamma(5/2)} \left(\frac{5}{2\sigma^2}\right)^{5/2} \exp\left(-\frac{5\delta_l^2}{2\sigma^2} + \frac{15I}{2\sigma^2}\right) \\ &\quad \times (\lambda_1 - \lambda_2)(\lambda_2 - \lambda_3)(\lambda_1 - \lambda_3), \end{aligned} \tag{4}$$

where the final expression for p_0 is from Doroshkevich (1970), and I is the sum of the three permutations of $\lambda_i\lambda_j$ where $i \neq j$. Therefore, the joint distribution of λ_j in the $f_{\rm nl}$ model is

$$p(\boldsymbol{\lambda}|\sigma) = p(\delta_l|\sigma)\, p(\boldsymbol{\lambda}|\delta_l, \sigma) = p(\delta_l|\sigma)\, p_0(\boldsymbol{\lambda}|\delta_l, \sigma), \tag{5}$$

where $p(\delta_l|\sigma)$ is the distribution of the linear overdensity in the $f_{\rm nl}$ model, and $p_0(\boldsymbol{\lambda}|\delta_l, \sigma)$ is really a function of λ_i/σ and δ_l/σ. For the $f_{\rm nl}$ values of current interest, $p(\delta_l|\sigma)$ is only weakly non-Gaussian, so it can be approximated by the Edgeworth expansion (e.g. Lam & Sheth 2009, who also discuss the limitations of this approximation). Hence, the joint distribution of λ_j is

$$p(\boldsymbol{\lambda}|\sigma) = \left[1 + \frac{\sigma S_3}{6} H_3(\delta_l/\sigma)\right]\; p_0(\boldsymbol{\lambda}|\sigma), \tag{6}$$

where $H_3(\delta_l/\sigma) = (\delta_l/\sigma)^3 - 3(\delta_l/\sigma)$ is the Hermite polynomial. The dependence on $f_{\rm nl}$ is encoded in the skewness parameter σS_3 (e.g. Scoccimarro et al. 2004, and note that our convention means that S_3 is of same sign to $f_{\rm nl}$). As a result, equation (3) becomes

$$\begin{aligned} \rho_s\, p(\rho_s|V)\, {\rm d}\rho_s = \int {\rm d}\boldsymbol{\lambda}\, {\rm d}\boldsymbol{e} \left[1 + \frac{\sigma S_3}{6} H_3(\delta_l/\sigma)\right] \\ \times\; p_0(\boldsymbol{\lambda}|\sigma)\, \delta_{\rm D}\left[\rho_s = \rho_s'(\boldsymbol{\lambda}, \boldsymbol{e})\right]. \end{aligned} \tag{7}$$

Except for the term in square brackets (the Edgeworth correction factor), the quantity in the integral is the same as in the Gaussian case. If we think of this extra factor as a weight, then the resulting non-linear redshift PDF in the $f_{\rm nl}$ model is just a suitably weighted version of that in the Gaussian case. The weight depends on σS_3, i.e. on $f_{\rm nl}$.

We can gain some intuitive understanding of the effect of a non-zero $f_{\rm nl}$ as follows. For $f_{\rm nl} = -100, \sigma S_3 < 0$ so that overdense regions are suppressed compared to the Gaussian case (the weight factor is less than unity), whereas underdense regions are enhanced compared to the Gaussian case (the weight factor is larger than unity). Finally, note that $|\sigma S_3| \ll 1$; on Mpc scales $\sigma S_3 \approx -0.03$ for $f_{\rm nl} = -100$, and it is a weakly decreasing function of scale (e.g. Scoccimarro et al. 2004). This will be important in what follows.

2.2 Ellipsoidal collapse and the non-linear overdensity

The next step is to estimate how ρ_s depends on $(\boldsymbol{\lambda}, e)$. In real space, the ellipsoidal evolution model sets

$$\rho_r \equiv \prod_{j=1}^{3} \frac{R_j^i}{R_{\rm E}} \approx \frac{(1-\delta_l/3)^3}{(1-\delta_l/\delta_{\rm c})^{\delta_{\rm c}}} \prod_{j=1}^{3}(1-\lambda_j)^{-1}, \tag{8}$$

(Lam & Sheth 2008a), where R_j^i are the initial lengths of the patch which is now an sphere of radius $R_{\rm E}$, and $\delta_{\rm c}$ is the critical value of spherical collapse model (its exact value depends weakly on cosmology: $\delta_{\rm c} \approx 1.66$ for the Λ cold dark matter (ΛCDM) cosmology for which we show simulation data in the next section). In redshift space, the model sets

$$\frac{\rho_s}{\rho_r} \approx \left[1 - \sum_{k=1}^{3} \frac{f\left\{R_k^i\lambda_k - A_h^i\delta_l\left[1-(1-\delta_l/\delta_{\rm c})^{\delta_{\rm c}/3-1}\right]/3\right\}}{R_k^i(1-\lambda_k) - A_h^i\left[1-\delta_l/3-(1-\delta_l/\delta_{\rm c})^{\delta_{\rm c}/3}\right]} e_k^2\right]^{-1}, \tag{9}$$

(Lam & Sheth 2008b), where $f = {\rm d}\ln D/{\rm d}\ln a$ with $D(t)$ the linear growth factor, $(e_1, e_2, e_3) = (\cos\psi\ \sin\theta, \sin\psi\ \sin\theta, \cos\theta)$, and $A_h^i \equiv 3/\sum_j (R_k^i)^{-1}$, where the R_j^i are the initial axis lengths.

2.3 Non-linear PDF in redshift space

Equations (3) and (9) are the bases for the computation of the non-linear redshift space PDF. The analysis simplifies considerably if we approximate σS_3 as a constant for a given Eulerian smoothing scale (recall that the scale dependence is rather weak): $\sigma S_3(r_0, \rho_s) \approx \sigma S_3(r_0)$. With this assumption, we can write equation (3) as

$$\begin{aligned}\rho_s\, p(\rho_s|V){\rm d}\rho_s &= \int {\rm d}\boldsymbol{\lambda}\, {\rm d}\boldsymbol{e}\; p(\boldsymbol{\lambda}|1)\, \delta_{\rm D}\left[\rho_s = \rho_s'(\sigma\boldsymbol{\lambda}, \boldsymbol{e})\right] \\ &= \int {\rm d}\boldsymbol{\lambda}\, {\rm d}\boldsymbol{e}\left[1 + \frac{\sigma S_3}{6} H_3(\delta_l)\right] \\ &\quad \times\; p_0(\boldsymbol{\lambda}|1)\, \delta_{\rm D}\left[\rho_s = \rho_s'(\sigma\boldsymbol{\lambda}, \boldsymbol{e})\right].\end{aligned} \tag{10}$$

In practice, we construct the PDF by Monte Carlo solution of the integral. This is straightforward because the six independent components of the deformation tensor $\Phi_{ij} = \partial_i\partial_j\Phi$ can be combined in the form $C = \{x, y, z, \Phi_{12}, \Phi_{23}, \Phi_{31}\}$, where

$$x = \sum_i \Phi_{ii},\ y = \frac{\Phi_{11} - \Phi_{22}}{2},\ z = \frac{\Phi_{11} + \Phi_{22} - 2\Phi_{33}}{2}. \tag{11}$$

The reason for doing this is that, to the second order in $f_{\rm nl}$, only x has non-zero skewness (Lam et al. 2009). Therefore, we can draw the other five parameters from Gaussian distributions with variance

$$\langle y^2\rangle = \langle\Phi_{ij}^2\rangle_{i\neq j} = \frac{\sigma^2}{15} \quad \text{and} \quad \langle z^2\rangle = \frac{\sigma^2}{5}. \tag{12}$$

The parameter x is drawn from an Edgeworth distribution. The associated $(\lambda_1, \lambda_2, \lambda_3)$ can be computed by solving the eigenvalue problem and the non-linear redshift PDF is then evaluated using equation (10).

In the next section, we compare this full solution with measurements in simulations. Note however that, in the limit $\rho_s - 1 \ll 1$, the non-linear redshift space PDF can be solved perturbatively. Appendix A provides details and shows that, to the lowest order, the variance in the redshift space counts is related to that in real space by Kaiser's formula for $f_{\rm nl} = 0$; the dependence on $f_{\rm nl}$ enters at higher order.

3 COMPARISON WITH SIMULATIONS

We now compare the predictions of our model with measurements of the non-linear PDF in numerical simulations from Desjacques et al. (2009). The numerical simulations followed the evolution of 1024^3 particles in a periodic cube of sides $1600h^{-1}$ Mpc. The background cosmology was ΛCDM with $(\Omega_{\rm m}, \Omega_{\rm b}, n_s, h, \sigma_8) = (0.279, 0.0462, 0.96, 0.7, 0.81)$.

Fig. 1 compares our model with the measured redshift space PDF of counts in $8\,h^{-1}$ Mpc spheres. In the upper panel, the solid symbols show the PDF for $f_{\rm nl} = 0$. We have not shown results for $f_{\rm nl} = \pm 100$ in that panel since they only slightly differ from the Gaussian case. Instead, the symbols in the bottom panel show the fractional deviation in these models relative to the Gaussian case. Filled and open symbols are for $f_{\rm nl} = 100$ and -100, respectively. As we can see, a positive $f_{\rm nl}$ slightly skews the PDF towards overdense regions. Conversely, the fraction of underdense regions is enhanced for negative $f_{\rm nl}$. In this respect, the redshift space PDF shows the same qualitative dependence on $f_{\rm nl}$ as the real space PDF, as expected (c.f. discussion following equation 7).

The dashed, solid and dotted curves in the top panel show the predictions for $f_{\rm nl} = 100, 0$ and -100, respectively. The differences are small, so the curves appear almost identical, but the bottom panel shows that they are indeed slightly different from one another and that our model provides a good description of the ratios, except in the high-density tail where it underpredicts the dependence on $f_{\rm nl}$. Note however that, in this strongly non-linear regime, our model drastically overpredicts the Gaussian counts.

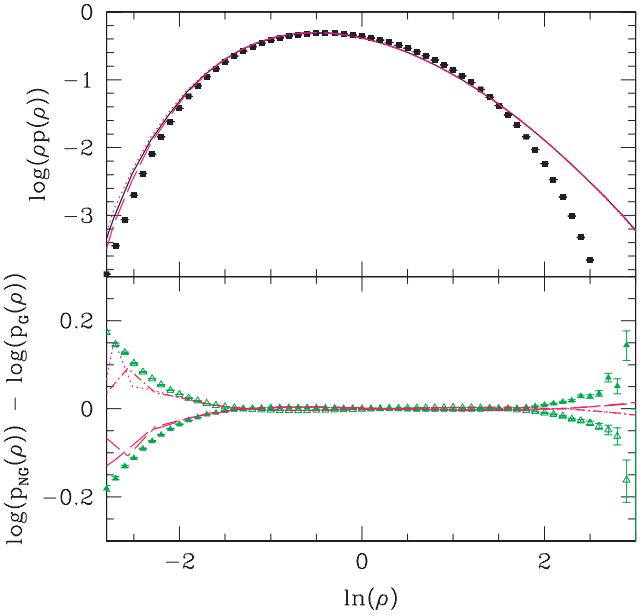

Figure 1. Comparisons of the measured PDF with our model for counts in $8\,h^{-1}$ Mpc sphere. The upper panel shows $\log[\rho\, p(\rho)]$ against $\ln(\rho)$ for the measured PDF (solid symbols, $f_{\rm nl} = 0$) and the theoretical prediction obtained by evaluating the non-linear PDF equation (3) for $f_{\rm nl} = 0$ (black, solid), -100 (magenta, dotted) and 100 (magenta, dashed), respectively. The lower panel shows the logarithm of the ratio between the $f_{\rm nl} \neq 0$ and Gaussian counts. The filled and empty symbols indicate the measurement for $f_{\rm nl} = 100$ and -100, respectively. The predictions obtained by applying the Edgeworth expansion weighting are represented by the dot–dashed (red, $f_{\rm nl} = -100$) and the short–long-dashed (red, $f_{\rm nl} = 100$), respectively.

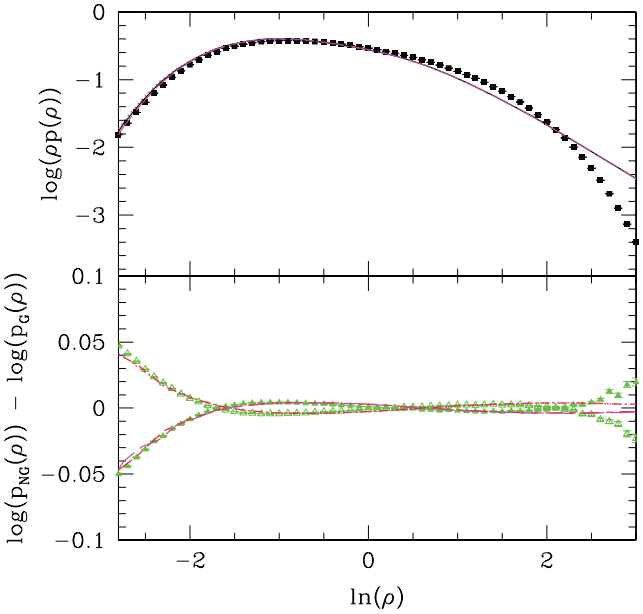

Figure 2. Same as Fig. 1, but for counts in spheres of radius $4h^{-1}$ Mpc.

We believe we understand why our model is more successful at predicting the ratio than the counts themselves. This is because at least some of the discrepancy at $\rho_s \gg 1$ arises from the fact that the highly non-linear virial motions within haloes will act to erase large density contrasts – these motions are *not* part of our model. Figs 1 and 2 in Lam & Sheth (2008b) show that, for $f_{\rm nl} = 0$, virial motions reduce the $\rho_s \gg 1$ tail, enhance the intermediate $\rho_s \sim 2$ region of the PDF, and have almost no effect on the $\rho_s < 0$ regime. Removing virialized motions within haloes from the measurements substantially reduces the discrepancy between theory and the simulations at $\rho_s > 0$. Although virial motions do not depend on $f_{\rm nl}$, their net effect depends upon the halo mass function. Since the later does depend on $f_{\rm nl}$, we may thus expect a slightly stronger suppression when $f_{\rm nl} > 0$ (as the abundance of massive haloes is slightly enhanced). On the other hand, the real space PDF, which is also affected by virial motions, has a more pronounced high-density tail for $f_{\rm nl} > 0$. As a result, the ratio of non-Gaussian counts to Gaussian counts depends only weakly on $f_{\rm nl}$. Therefore, our model can provide a reasonable description of the ratio even though it fails at describing the high-ρ_s tail of the Gaussian density PDF.

Fig. 2 shows a similar comparison on smaller scales (spheres of radius $4\,h^{-1}$ Mpc). The dependence on $f_{\rm nl}$ is smaller compared with the previous figure. Our model still provides a good description of the ratio relative to the $f_{\rm nl} = 0$ counts, except at the highest densities where it overpredicts the $f_{\rm nl} = 0$ counts and underpredicts the ratio. Note again that we expect much of this discrepancy to be reduced if we were to remove virial motions from the simulations.

4 DISCUSSION

We used the ellipsoidal evolution model to study the redshift space PDF of the non-linear dark matter density field in the local non-Gaussian $f_{\rm nl}$ model.

A perturbative analysis of the density PDF equation (3) shows that, at the lowest order, Kaiser's formula still holds in the $f_{\rm nl}$ model (although his original derivation does not assume Gaussianity explicitly, other derivations of the formula have done so as discussed in the Introduction). The effects of $f_{\rm nl} \neq 0$ appear in the first-order corrections to the variance (and higher order moments). One could, therefore, constrain $f_{\rm nl}$ from large-scale structure by measuring the variance and the higher order moments and comparing with the perturbative quantities in Section A (with some dynamical models to determine ν_i).

Our approach remains accurate on smaller scales where perturbative treatments are not useful. Simulations show that the dependence on $f_{\rm nl}$ is qualitatively similar to that for the real space PDF: for positive $f_{\rm nl}$ (positive σS_3) both PDFs skew slightly towards overdense regions. In addition both show stronger $f_{\rm nl}$ dependence in the underdense regions, suggesting that void abundances should be good probes for primordial non-Gaussianity (e.g. Kamionkowski et al. 2009; Lam et al. 2009). Our model (equation 7) captures these trends (Figs 1 and 2). Since it is explicitly a redshift space calculation, it would be interesting to see if it correctly predicts the $f_{\rm nl}$ dependence of the PDF of the flux in the Lyα forest, that has recently been simulated by Viel et al. (2009). This work also provides the foundation for constraining $f_{\rm nl}$ in future galaxy surveys [e.g. the change in the redshift space halo/galaxy power spectrum by combining with the scale-dependent halo/galaxy bias (Dalal et al. 2008; Desjacques et al. 2009; Slosar 2009)].

ACKNOWLEDGMENTS

VD acknowledges support from the Swiss National Foundation under contract No. 200021-116696/1. RKS was supported in part by NSF-AST 0908241. TYL was partly supported by World Premier International Research Center Initiative (WPI Initiative), MEXT, Japan.

REFERENCES

Afshordi N., Tolley A. J., 2008, Phys. Rev. D, 78, 123507
Bernardeau F., 1994, A&A, 291, 697
Bernardeau F., Colombi S., Gaztañaga E., Scoccimarro R., 2002, Phys. Rep., 367, 1
Bond J. R., Myers S. T., 1996, ApJS, 103, 1
Buchbinder E. I., Khoury J., Ovrut B. A., 2008, Phys. Rev. Lett., 100, 171302
Carbone C., Verde L., Matarrese S., 2008, ApJ, 684, L1
Dalal N., Doré O., Huterer D., Shirokov A., 2008, Phys. Rev. D, 77, 123514
Desjacques V., 2008, MNRAS, 388, 638
Desjacques V., Sheth R. K., 2009, preprint (arXiv:0909.4544)
Desjacques V., Seljak U., Iliev I. T., 2009, MNRAS, 396, 85
Doroshkevich A. G., 1970, Astrofizika, 6, 581
Fisher K. B., 1995, ApJ, 448, 494
Grossi M., Branchini E., Dolag K., Matarrese S., Moscardini L., 2008, MNRAS, 390, 438
Grossi M., Verde L., Carbone C., Dolag K., Branchini E., Iannuzzi F., Matarrese S., Moscardini L., 2009, MNRAS, 398, 321
Hikage C., Matsubara T., Coles P., Liguori M., Hansen F. K., Matarrese S., 2008, MNRAS, 389, 1439
Hivon E., Bouchet F. R., Colombi S., Juszkiewicz R., 1995, A&A, 298, 643
Izumi K., Soda J., 2007, Phys. Rev. D, 76, 083517
Jeong D., Komatsu E., 2009, ApJ, 703, 1230
Kaiser N., 1987, MNRAS, 227, 1
Kamionkowski M., Verde L., Jimenez R., 2009, J. Cosmol. Astropart. Phys., 1, 10
Khoury J., Piazza F., 2009, JCAP, 07, 026
Komatsu E. et al., 2009, ApJS, 180, 330
Koyama K., Soda J., Taruya A., 1999, MNRAS, 310, 1111

Lam T. Y., Sheth R. K., 2008a, MNRAS, 389, 1249
Lam T. Y., Sheth R. K., 2008b, MNRAS, 386, 407
Lam T. Y., Sheth R. K., 2009, MNRAS, 395, 1743
Lam T. Y., Sheth R. K., Desjacques V., 2009, MNRAS, 399, 1482
Lo Verde M., Miller A., Shandera S., Verde L., 2008, J. Cosmol. Astropart. Phys., 4, 14
Manera M., Sheth R. K., Scoccimarro R., 2009, MNRAS, in press (arXiv:0906.1314)
McDonald P., 2008, Phys. Rev. D, 78, 123519
McEwen J. D., Hobson M. P., Lasenby A. N., Mortlock D. J., 2008, MNRAS, 388, 659
Matarrese S., Verde L., 2008, ApJ, 677, L77
Matarrese S., Verde L., Jimenez R., 2000, ApJ, 541, 10
Ohta Y., Kayo I., Taruya A., 2004, ApJ, 608, 647
Pillepich A., Porciani C., Hahn O., 2008, preprint (arXiv:0811.4176)
Rossi G., Sheth R. K., Park C., Hernandez-Monteagudo C., 2009, MNRAS, 399, 304
Scoccimarro R., Frieman J. A., 1999, ApJ, 520, 35
Scoccimarro R., Sefusatti E., Zaldarriaga M., 2004, Phys. Rev. D, 69, 103513
Sefusatti E., Komatsu E., 2007, Phys. Rev. D, 76, 083004
Sheth R. K., Mo H. J., Tormen G., 2001, MNRAS, 323, 1
Silvestri A., Trodden M., 2008, preprint (arXiv:0811.2176)
Slosar A., 2009, J. Cosmol. Astropart. Phys., 3, 4
Slosar A., Hirata C., Seljak U., Ho S., Padmanabhan N., 2008, J. Cosmol. Astropart. Phys., 8, 31
Taruya A., Koyama K., Matsubara T., 2008, Phys. Rev. D, 78, 123534
Viel M., Branchini E., Dolag K., Grossi M., Matarrese S., Moscardini L., 2009, MNRAS, 393, 774
Yadav A. P. S., Wandelt B. D., 2008, Phys. Rev. Lett., 100, 181301

APPENDIX A: PERTURBATIVE TREATMENT OF REDSHIFT SPACE DISTORTIONS

Equation (5) allows for a novel estimate of how redshift space statistics are expected to differ from those in real space as $f_{\rm nl}$ varies. This is because the overdensity in redshift space is

$$1+\delta_s \approx 1+\delta_s^{(1)}+\delta_s^{(2)}+\delta_s^{(3)}+\cdots, \tag{A1}$$

where

$$\delta_s^{(1)} = \delta_r^{(1)} + \Delta_z^{(1)}$$

$$\delta_s^{(2)} = \delta_r^{(2)} + \Delta_z^{(2)} + \delta_r^{(1)}\,\Delta_z^{(1)}$$

$$\delta_s^{(3)} = \delta_r^{(3)} + \Delta_z^{(3)} + \delta_r^{(2)}\,\Delta_z^{(1)} + \delta_r^{(1)}\,\Delta_z^{(2)}, \tag{A2}$$

with

$$\delta_r{}^{(1)} = \sum_{j=1}^{3}\lambda_j$$

$$\delta_r{}^{(2)} = \frac{\nu_2}{2}\,\delta_l^2 + \frac{\delta_l^2}{3} - \sum_{j\neq k}\lambda_j\lambda_k$$

$$\delta_r{}^{(3)} = \frac{\nu_3}{6}\,\delta_l^3 + \frac{17}{27}\,\delta_l^3 - 2\delta_l\sum_{j\neq k}\lambda_j\lambda_k - 5\lambda_1\lambda_2\lambda_3, \tag{A3}$$

and

$$\begin{aligned}
\Delta_z^{(1)} &= f_1\sum_{k=1}^{3}\lambda_k\,e_k^2\\
\Delta_z^{(2)} &= f_1\sum_{k=1}^{3}\left[\frac{\nu_2}{2}\,\frac{f_2}{f_1}-\frac{4}{3}\right]\frac{\delta_l^2}{3}\,e_k^2 + f_1^2\sum_{k=1}^{3}\lambda_k^2\,e_k^2\\
&\quad + f_1^2\sum_{j,k=1}^{3}\lambda_j\lambda_k\,e_j^2e_k^2\\
\Delta_z^{(3)} &= f_1\sum_{k=1}^{3}\frac{\delta_l^2}{3}\left[\left(\frac{\nu_2}{2}\,\frac{f_2}{f_1}-\frac{4}{3}\right)\lambda_k\right.\\
&\quad \left.+\left(\frac{\nu_3}{6}\,\frac{f_3}{f_1}-\frac{2\nu_2}{3}-\frac{5\nu_2}{6}\,\frac{f_2}{f_1}+2\right)\delta_l\right]e_k^2\\
&\quad + 2f_1^2\sum_{j,k=1}^{3}\lambda_j\left[\left(\frac{\nu_2}{2}\,\frac{f_2}{f_1}-\frac{4}{3}\right)\frac{\delta_l^2}{3}+\lambda_k^2\right]e_j^2e_k^2\\
&\quad + f_1^3\sum_{i,j,k=1}^{3}\lambda_i\lambda_j\lambda_k\,e_i^2e_j^2e_k^2,
\end{aligned} \tag{A4}$$

(Lam & Sheth 2008b). Here, $f_1 = {\rm d}\ln D_1/{\rm d}a \approx \Omega^{0.55}$ where D_1 is the linear growth factor, $f_2 = {\rm d}\ln D_2/{\rm d}a$ where $D_2/D_1^2 \approx -(3/7)\Omega^{-1/143}$ and $\nu_2 \approx 1.62$ and $\nu_3 \approx 3.93$ are related to the spherical evolution model.

Note that setting $f_{\rm nl}\neq 0$ simply changes the values of the averages over the λs. Hence, to the lowest order,

$$\begin{aligned}
\langle\delta_s^2\rangle &\approx \langle(\delta_s^{(1)})^2\rangle = \langle(\delta_r^{(1)})^2 + 2\delta_r^{(1)}\Delta_z^{(1)} + (\Delta_z^{(1)})^2\rangle\\
&= \sigma^2 + \frac{2f_1}{3}\,\sigma^2 + \frac{f_1^2}{15}\left\langle(3\delta^2-4I)\right\rangle\\
&= \left(1+\frac{2}{3}f_1\right)\sigma^2 + \frac{f_1^2}{15}\left\langle\frac{5\delta^2}{3}+\frac{4}{3}(\delta^2-3I)\right\rangle\\
&= \left(1+\frac{2}{3}f_1+\frac{f_1^2}{9}+\frac{4f_1^2}{45}\right)\sigma^2\\
&= \left(1+\frac{2}{3}f_1+\frac{f_1^2}{5}\right)\sigma^2;
\end{aligned} \tag{A5}$$

this is Kaiser's formula, so the relation between real and redshift space variance is unchanged from the Gaussian case.

Of course, $f_{\rm nl}$ matters for the higher order moments. The next higher order of the redshift-space variance is

$$\begin{aligned}
\langle\delta_s^2\rangle^{(2)} &= 2\langle\delta_s^{(1)}\delta_s^{(2)}\rangle\\
&= 2\left\langle\delta_r^{(1)}\delta_r^{(2)} + \delta_r^{(1)}\Delta_z^{(2)} + \delta_r^{(1)2}\Delta_z^{(1)} + \Delta_z^{(1)}\delta_r^{(2)}\right.\\
&\quad \left.+\,\Delta_z^{(1)}\Delta_z^{(2)} + \delta_r^{(1)}\Delta_z^{(1)2}\right\rangle\\
&= 2\frac{\sigma S_3}{6}\sigma^3\left[3\nu_2+\left(\nu_2+\frac{2}{3}\right)f_1 - \frac{44}{45}f_1^2 + \frac{4}{9}f_1^3\right.\\
&\quad \left.+\;\frac{\nu_2}{3}f_1f_2 + \nu_2 f_2\right].
\end{aligned} \tag{A6}$$

The origin of these terms can be understood as follows. When $f_{\rm nl}=0$, then one can think of the three terms in Kaiser's expression as being due to the density–density, density–velocity and velocity–velocity power spectra. Now, velocities are related to first derivatives of the potential, whereas densities are related to second derivatives. So one expects the lowest order corrections to the Gaussian result to scale as $f_{\rm nl}$. Terms in the first-order correction (second equality in equation A.6) can be interpreted as $B_{ddd}, B_{dvv}, B_{ddv}, B_{ddv}, B_{vvv}$ and

B_{dvv}, respectively, where B denotes bispectra, d and v are density and velocity. Notice that this first-order correction in the redshift variance is of lower order compared with the case where $f_{\rm nl} = 0$ (and hence $\sigma\ S_3 = 0$). This is generic for models with non-vanishing initial skewness (Bernardeau et al. 2002).

This approach can be extended to estimate the real-redshift large-scale relation in higher order statistics, for example the bispectrum of galaxies to constrain $f_{\rm nl}$ (see e.g. Scoccimarro et al. 2004 or more recently Jeong & Komatsu 2009). However, complications arise when one includes scale-dependent halo/galaxy bias (Dalal et al. 2008; Desjacques et al. 2009; Desjacques & Sheth 2009; Slosar 2009) and the validity of the peak-background split approach in computing halo bias (Manera, Sheth & Scoccimarro 2009). These are beyond the scope of this paper and will be explored in future studies.

This paper has been typeset from a TEX/LATEX file prepared by the author.